Coiling of a viscoelastic fluid filament

Yunxing Su,[1] Bernardo Palacios,[2] and Roberto Zenit[1,2,*]

[1]*Center for Fluid Mechanics, School of Engineering, Brown University, Providence, Rhode Island 02912, USA*

[2]*Instituto de Investigaciones en Materiales, Universidad Nacional Autónoma de México, Apdo. Postal 70-360, Ciudad Universitaria, D.F. 04510, México*

(Received 27 October 2020; accepted 1 March 2021; published 18 March 2021)

A viscous filament falling from a certain height onto a surface can form coils resulting from a buckling instability. This coiling phenomenon has been extensively studied for Newtonian fluids. However, the effect of liquid viscoelasticity has not been fully explored. Here we present experimental measurements of the coiling performance using Newtonian fluids and viscoelastic Boger fluids. Compared to Newtonian fluids with a comparable viscosity, the onset of viscoelastic fluid coiling is delayed; the coiling frequency is found to be smaller for viscoelastic fluids under the same experimental conditions. We show that these differences in coiling performance are due to the prevalence of extensional viscosity in viscoelastic fluids. Moreover, we find that the coiling frequency curves of different Newtonian fluids can be collapsed using a gravitational frequency and length scaling. This frequency and length scaling can also be used to collapse the data for Boger fluids considering the extensional viscosity instead of shear viscosity, confirming the importance of this property on filament coiling phenomenon for viscoelastic liquids.

DOI: 10.1103/PhysRevFluids.6.033303

I. INTRODUCTION

A viscous fluid filament issues from a nozzle toward a flat horizontal wall from a certain height. If the fluid is sufficiently viscous, its deposition onto the surface is characterized by a coiling motion: the fluid filament coils around its own axis with a frequency Ω and radius R. As it coils, a helical structure of fluid is formed directly over the contact point on the liquid pool. The instability was first described by Barnes and Woodcock [1], who coined the name "liquid rope coiling." Taylor [2] hypothesized that the buckling of fluid filaments was due to the presence of longitudinal compression of the thread and in this sense was a hydrodynamic analog of Eulerian instability in thin elastic rods. Tchavdarov *et al.* [3] applied linear stability analysis to examine the onset of the fluid filament coiling, confirming Taylor's hypothesis. Cruickshank [4] experimentally studied the onset of the viscous filament coiling including the effect of surface tension. The authors found that the surface tension effects were negligible compared with the large viscosity of the fluids, i.e. for large capillary numbers, $\mathrm{Ca} = \mu U/\sigma$, where U is the fluid velocity within the filament, μ is the shear viscosity and σ is the surface tension.

Ribe [5] and Ribe *et al.* [6] developed a numerical model of a thin 'liquid rope' and found four distinct coiling modes (viscous, gravitational, inertial-gravitational and inertial modes) based on the force balance in the coiling filament. These four coiling modes were then confirmed by experimental observations [7,8]. Ribe *et al.* [9] made an extensive review of the Newtonian coiling phenomena and other novel phenomena related to it. And more recently Ribe [10] further completed the understanding of the problem by considering normalized variables to describe the entire regime

*zenit@brown.edu

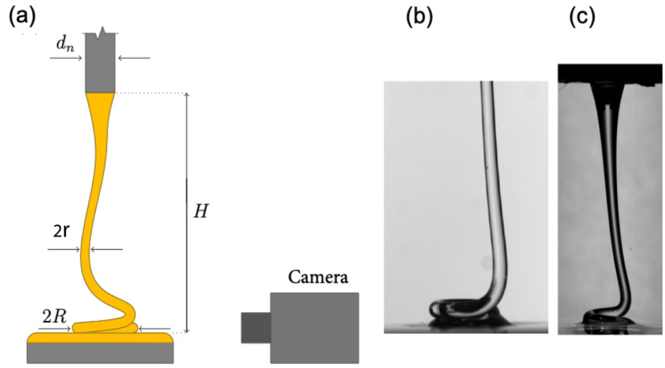

FIG. 1. (a) Scheme of the experimental setup: viscous fluids released from a nozzle (diameter, d_n) located above the bottom plate. Typical images of a viscous filament coiling: (b) Boger fluid and (c) Newtonian fluid.

diagram for the Newtonian liquid rope coiling. Recent experimental work [11] developed a controllable test apparatus and reported a transition from gravitational mode to inertial mode without an inertial-gravitational mode in between by using Newtonian fluids.

An interesting related flow is the so-called "fluid mechanical sewing machine" [12,13]. In that case the liquid filament coils onto a substrate that moves at a constant linear speed. Consequently, the fluid coils spread as they fall, forming zig-zagging drawings of different topologies. The recent paper by Palacios *et al.* [14] argued that Jackson Pollock, the famous American abstract expressionist painter, purposely avoided the coiling instability to paint with his dripping technique.

Most of the literature on viscous filament coiling concerns Newtonian fluids. Non-Newtonian fluids, in general, can significantly modify the way in which fluids flow. In the particular case of filaments, one of the examples is the famous Kaye effect (leaping-shampoo effect), in which the falling shear-thinning fluids leap up from the deposited fluids on the bottom plate [15–18]. Majmudar *et al.* [19] surveyed the complex nonlinear dynamics of a coiling filament, including the Kaye effect using shear-thinning viscoelastic fluids. Their paper, to our knowledge, was the first to address the effect of viscoelasticity on coiling phenomenon. However, an in-depth understanding of its nature was not offered.

To understand the viscoelastic effect in viscous filament coiling, we use Boger fluids in the present study, which are viscoelastic but have a nearly constant viscosity [20]. For validation and reference, we also test the coiling performance with Newtonian fluids (corn syrup/water solutions) of comparable viscosity to Boger fluids. In the present study, we first in Sec. III A examine the coiling performance of Newtonian fluids using a gravitational frequency and length scale to correctly normalize the data. Then in Sec. III B we extend the scaling to viscoelastic Boger fluids and propose the use of extensional viscosity, instead of shear viscosity, in the gravitational scaling to collapse the frequency curves for viscoelastic fluids. Then independent measurements of extensional viscosity are presented, validating the proposed use of extensional viscosity. In Sec. III C we discuss the connection between the coiling frequency and the coiling radius with special attention on the frequency jump in the coiling frequency curves.

II. EXPERIMENTAL PROCEDURE

Figure 1(a) shows a sketch of the experimental setup. A syringe pump is used to create a fluid thread with a constant flow rate Q. The thread exits from a nozzle of diameter d_n, and falls from a certain height H onto a solid surface. The process is recorded by a digital camera and image processing is used to determine the thread radius r, the coiling frequency Ω, and the coiling radius R. Very similar setups have been used for the study of Newtonian fluid coiling (e.g., Habibi *et al.* [8]). Figures 1(b) and 1(c) show images of typical experiments conducted on the described setup

TABLE I. Composition in weight percentage of the prepared fluids: including Newtonian fluids N1, N2, and N3, and Boger fluids B1, B2, B3, B4, and B5 with different PAA percentages in weight.

Fluids	PAA in water %	PAA solution %	Glucose %
N1	0	5	95
N2	0	7.5	92.5
N3	0	10	90
B1	0.05	10	90
B2	0.10	10	90
B3	0.15	10	90
B4	0.225	10	90
B5	0.30	10	90

for the two types of fluids considered in this study. In both cases, the viscous fluid filament coils to form a stack of fluids on a flat plate.

Test fluids and rheology

Newtonian and Boger fluids are tested in the present study. We use the mixture of corn syrup and water to make Newtonian fluids. With different percentages of water, we can fabricate Newtonian fluids with different viscosity (Tables I and II). Boger fluids are used in the present study, which have a nearly constant viscosity as well as a significant elasticity. Thus, Boger fluids offer a significant advantage to study the effects of viscoelasticity since shear-dependent viscosity effects can be neglected. Most non-Newtonian fluids exhibit both effects simultaneously, which complicates the interpretation of results. Boger fluids are often described by the Oldroyd-B material model [21], for which the steady shear material functions are

$$\tau = \mu\dot{\gamma}, \tag{1}$$

$$N_1 = \Psi\dot{\gamma}^2, \tag{2}$$

where $\dot{\gamma}$ is the shear rate, τ is the shear stress, μ is the shear viscosity, N_1 is the first normal stress and Ψ is the first normal stress index. The fluid elasticity can be quantified by the relaxation time λ,

$$\lambda = \frac{\Psi}{2\mu}. \tag{3}$$

TABLE II. Rheology of fluids tested in the present study, including Newtonian fluids N1, N2 and N3, and Boger fluids B1, B2, B3, B4, and B5.

Fluids	Viscosity μ (Pa s)	Kinematic viscosity ν (m^2/s)	Relaxation time λ (s)	Power index n
N1	20.4	14.5×10^{-3}	0	0.99
N2	14.4	10.2×10^{-3}	0	0.98
N3	4.1	2.9×10^{-3}	0	0.96
B1	5.6	3.9×10^{-3}	1.24×10^{-3}	0.95
B2	8.6	6.0×10^{-3}	2.24×10^{-3}	0.96
B3	9.4	6.6×10^{-3}	2.60×10^{-3}	0.95
B4	8.0	5.7×10^{-3}	9.55×10^{-3}	0.96
B5	20.0	1.4×10^{-2}	1.50×10^{-2}	0.96

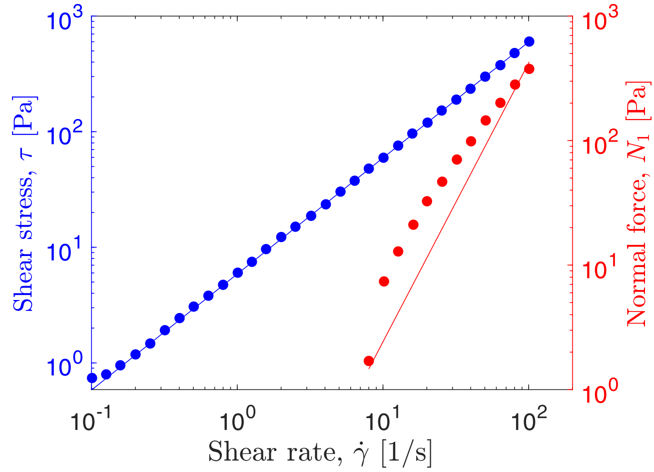

FIG. 2. Shear stress τ and normal stress N_1 for glucose-water-PAA Boger fluids B1. Shear stress data are fitted to a power-law model (blue line); the viscosity is nearly constant since $n \in [0.9, 1]$. Normal stress data are fitted to a quadratic normal stress behavior (red line).

Different Boger fluids were fabricated for this study. The fluids consisted of distilled water, glucose (corn syrup, Golden Barrel, and La Gloria 43°), and polyacrylamide (PAA, Sigma Aldrich with molecular weight $M_w = 5 \times 10^6$). This recipe is well known and has been used in several previous works [20,22–25]. The water-glucose-PAA fluids have the advantage of being water soluble and therefore relatively easy to prepare and handle. To prepare the fluids, PAA was dissolved into water in a beaker with a magnetic stirrer. The solution was stirred at the maximum possible speed before spilling liquid off the vessel; this was done for at least 12 h. Once the PAA was well dissolved, glucose was added to the beaker. The liquid was then transferred into a mixer with an overhead stirrer at the lowest possible speed (approximately 10 RPM) with a low-shear stirring impeller (soft semiflexible long paddles) for at least 72 h.

The composition of the tests fluids is shown in Table I. The first column shows the amount of PAA used in the water-PAA solution, the second and third columns show the amount of water-PAA solution and glucose (in weight percentage), respectively, in the final mix.

Steady shear properties of the fluids were obtained with a rheometer (Ares-G2, TA Instruments). Tests were conducted with a cone-plate geometry (40 mm, 0.04 rad cone plate at 24 μm gap) at a temperature $T = 25\,^\circ$C. The steady shear tests of fluid B1 is shown in Fig. 2. Shear stress τ and first normal stress N_1 are plotted against shear rate $\dot{\gamma}$. The shear stress is fitted to a power law model $\tau = \mu_0 \dot{\gamma}^n$, where n is the power-law index. For all liquids n is very close to unity (see Table II), indicating a nearly constant shear viscosity μ ($\mu \approx \mu_0$). The first normal stress is fitted to a quadratic function of the shear rate to infer the first normal stress modulus Ψ [see Eq. (2)]; with it the relaxation time λ is obtained from Eq. (3).

To study the viscous filament coiling, for each fluid, we vary the nozzle height (fluid falling height), H, from which the fluid is ejected and falls onto a bottom plate, while the rest of parameters are kept constant throughout the experiment. The experimental parameters (range of falling height, flow rate, etc.) for each fluid can be found in Table III.

Note that surface tension effect is not expected to play a significant role in the present experiments. Considering that the capillary number is Ca $\sim O(10)$ and that the Bond number is Bo $\sim O(10^3)$ for all experiments, we can assume that the surface tension effect is small compared to the dominating forces (gravity, viscous and inertia forces). The Bond number is defined as Bo $= \rho g H^2/\sigma$. In addition, numerical studies of coiling filaments [5,26] show that the difference

TABLE III. Experimental parameters for each fluid: falling height, H, flow rate, Q, and nozzle diameter, d_n.

Fluids	H (mm) min	H (mm) max	Q (ml/min)	d_n (mm)
N1	25	210	9.8	6.35
N2	27	122	9.8	6.35
N3	32	201	9.8	6.35
B1	30	153	9.8	6.35
B2	56	292	9.8	6.35
B3	81	332	9.8	6.35
B4	81	404	9.8	6.35
B5	99	300	9.8	6.35

in steady coiling frequency is only a few percent between cases with and without considering the surface tension. Therefore, the surface tension effect is neglected.

III. RESULTS AND DISCUSSION

A. Filament coiling with Newtonian fluids

The viscous filament coiling using Newtonian fluids has been well studied and documented, either using silicone oil [5,8,10,26,27] or honey [11]. Considering a numerical approach, Ribe [10] identified four different coiling regimes: viscous, gravity, gravity-inertial, and inertial regimes. In the current experiment, we conducted similar Newtonian experiments considering corn syrup/water solutions. Adopting the length and frequency scaling from Ribe *et al.* [26], results of three Newtonian fluids are shown in Fig. 3 (gray triangles), including three corn syrup solutions. For validation purposes, we also compare our results with data from literature [colored triangles in Fig. 3(a)]. Similar to the results from others [8,11], in the current study we observed two regimes of filament coiling: a lower branch at small falling heights and a higher branch at large falling heights, with a frequency discontinuity (frequency jump) in between [Fig. 3(a)]. According to the analysis of

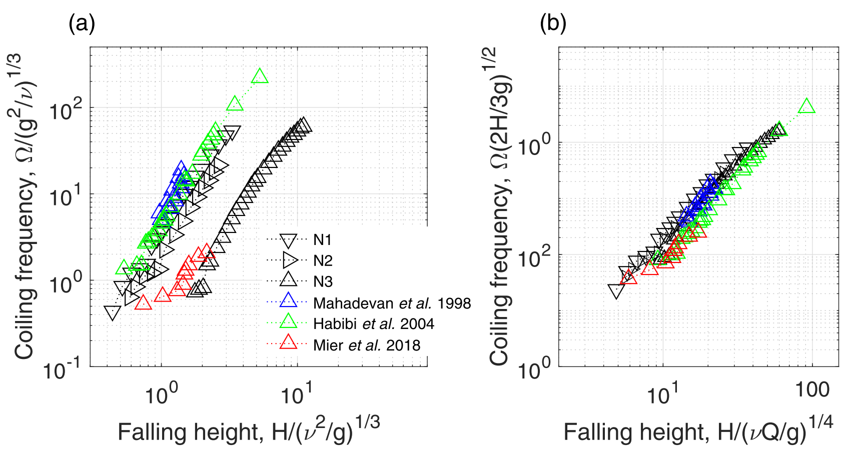

FIG. 3. Coiling frequency as a function of falling height for different experiments with Newtonian fluids (a) using the scaling from Ribe [10] and (b) using the scaling of Eq. (6) and single pendulum frequency. The nondimensional group (Π_1, Π_2) for the present Newtonian fluids are (103.3, 0.61), (71.7, 0.56), and (21.1, 0.41), respectively.

coiling modes from Ribe *et al.* [6], the lower branch is believed to fall in the gravity coiling mode while the higher branch is in the inertial mode, and the region around the frequency jump is in the inertial-gravity mode. We did not extend our measurements to observe the viscous mode in the current study. There is no significant decrease of the normalized coiling frequency at small falling heights, in accordance with previous experimental observations by Mier *et al.* [11] who reported only gravitational and inertial modes using honey as testing fluids. However, we also notice that this frequency jump happens at different falling heights for different fluids and flow rates: fluids with a lower viscosity tend to have a larger nondimensional falling height but a smaller nondimensional transition coiling frequency, suggesting that the scaling law in Fig. 3(a) is not sufficient to capture the frequency jump of the viscous filament coiling.

Considering an extended view of all the filament coiling parameters, Ribe *et al.* [6] proposed two nondimensional groups,

$$\Pi_1 = (\nu^5/gQ^3)^{1/5} \tag{4}$$

and

$$\Pi_2 = \left(\nu Q/g{d_n}^4\right)^{1/4}, \tag{5}$$

to characterize the filament coiling performance, where $\nu = \mu/\rho$ is kinematic shear viscosity, Q is flow rate and d_n is nozzle diameter. These authors pointed out that different coiling frequency curves were determined by different pairs of (Π_1, Π_2). In the current study, the frequency-height curves are in general similar in shape but do not collapse into one, which can be attributed to different pairs (Π_1, Π_2) in the experiments.

To understand the frequency jump, here we adopt a different scaling law that emphasizes the gravity effects since they play an important role in the viscous filament stretching and the resulting coiling frequency for the regime in which our measurements are located [6,28]. In particular, Ribe *et al.* [6] showed that the coiling filament in the inertial-gravity mode behaves like a whirling fluid string and the coiling frequency is proportional to the single pendulum frequency, $\Omega_0 = (g/H)^{1/2}$, where H is the falling height. This whirling-like string is also seen in the present study as shown in Fig. 1(c), where the filament coil includes most of the falling filament. Considering that the coiling filament resembles a compound conical pendulum, in the current study, we adopt a correction factor of $2/3$ for the effective falling height, which results in $\Omega_0 = (3g/2H)^{1/2}$ for the pendulum frequency scale.

Around the frequency jump (gravity mode) the viscous force is balanced by gravity force, $F_v \sim F_G$ [5], which results in a length scale,

$$\delta = (\nu Q/g)^{1/4}, \tag{6}$$

where ν is kinematic shear viscosity and Q is volumetric flow rate. As discussed in Ribe *et al.* [6], this length scale can be used to predict the falling height for the frequency jump in the frequency-height curves, which will be discussed in detail in Sec. III C.

Using the length scale [Eq. (6)] and the pendulum frequency scale (Ω_0), we nondimensionalize the falling height and the coiling frequency [Fig. 3(a)] and re-plot the results in Fig. 3(b). Under this scaling we can see that all the frequency-height curves collapse well for Newtonian fluids with different viscosity and flow rates, including those from literature. In particular, with this scaling the frequency jump occurs at the nondimensional frequency around 1, suggesting that the pendulum frequency scale captures the frequency jump for different fluids and flow rates.

B. Filament coiling with Boger fluids

In the previous section, we have showed that the scaling related to the gravitational mode works well in collapsing the frequency-height curves for different Newtonian fluids. In this section, we will extend this scaling to the coiling performance of Boger fluids, which are viscoelastic but have a nearly constant viscosity (see Table II). Experiments for Boger fluids were conducted in the same

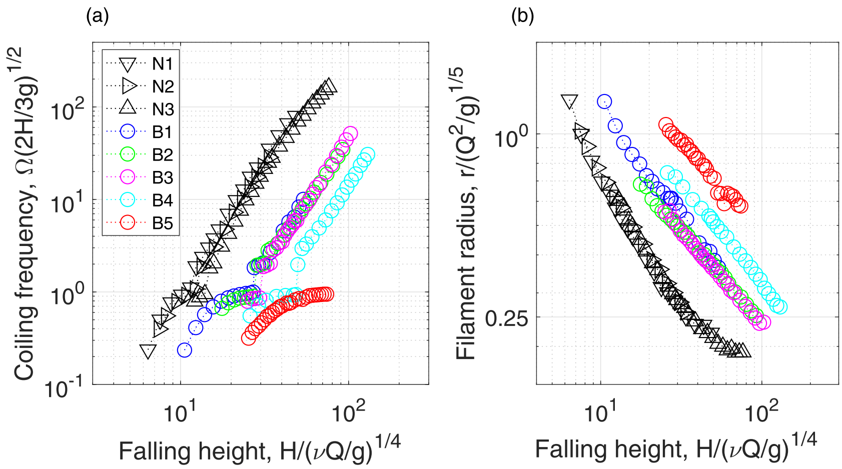

FIG. 4. (a) Filament coiling frequency and (b) filament radius as a function of falling height for both Newtonian and viscoelastic fluids; the falling height, H, is normalized by the kinematic shear viscosity ν.

way as Newtonian fluids. The results are shown in Fig. 4(a) together with the aforementioned Newtonian cases. We can see that similar to the Newtonian cases, most of the frequency-height curves for Boger fluids show two branches except the cases with the highest polymer concentration, which we believe is due to the height limitations in the experiment. It is to be noted that the frequency jump for all the fluids tested occurs at dimensionless frequency $\sim$1, indicating that the pendulum frequency scale is also appropriate for Boger fluids. This will be discussed in details later in Sec. III C.

However, in the horizontal axis the frequency-height curves of Boger fluids (circles) deviate from the Newtonian cases and shift to the right [Fig. 4(a)]: In general, as the polymer concentration increases, both the onset of filament coiling and the jump frequency are delayed and move to higher heights. Note that the fluid relaxation time also increases with the polymer concentration (see Table II). As discussed below, the change of behavior results from an increased value of the extensional viscosity, which is expected for Boger fluids. The extensional viscosity measures the fluid resistance to axial stretching and in literature is usually represented as the Trouton ratio, defined as the ratio between extensional and shear viscosities, $\mathrm{Tr} = \nu_e/\nu$. For Newtonian fluids, the Trouton ratio is constant and equal to 3; but for viscoelastic fluids, the Trouton ratio varies with the polymer concentration and can be of up to $\mathcal{O}(10^2)$ or $\mathcal{O}(10^3)$, much larger than the Newtonian counterpart [29]. Since the extensional viscosity is closely related to the filament stretching in addition to gravity and inertia [5], we anticipate that under the same experimental conditions, the filament radius will be wider for Boger fluids than Newtonian fluids. This is confirmed in Fig. 4(b), which shows the radius of the coiling filament for all the fluids tested. For a given dimensionless height, the filament radius increases with the relaxation time. The filament radius is normalized by a length scale characterized by the inertia (flow rate Q) and gravity effects.

Similar to the performance of coiling frequency, the filament radii of Newtonian fluids show a good collapse using the length scale of Eq. (6) [gray triangles in Fig. 4(b)], and they are in general smaller than the filament radii of Boger fluids at the same falling height. As the flow velocity within the filament can be estimated as $U \sim Q/\pi r^2$, a larger filament radius leads to a smaller fluid velocity in the filament at a constant flow rate. Also, when the filament coils, the coiling frequency can be estimated as $\Omega \sim U/R$, where R is filament coiling radius. As a result, the change in filament radius can eventually affect the coiling frequency, in agreement with the present observation of shifting coiling frequency curves in Fig. 4(a).

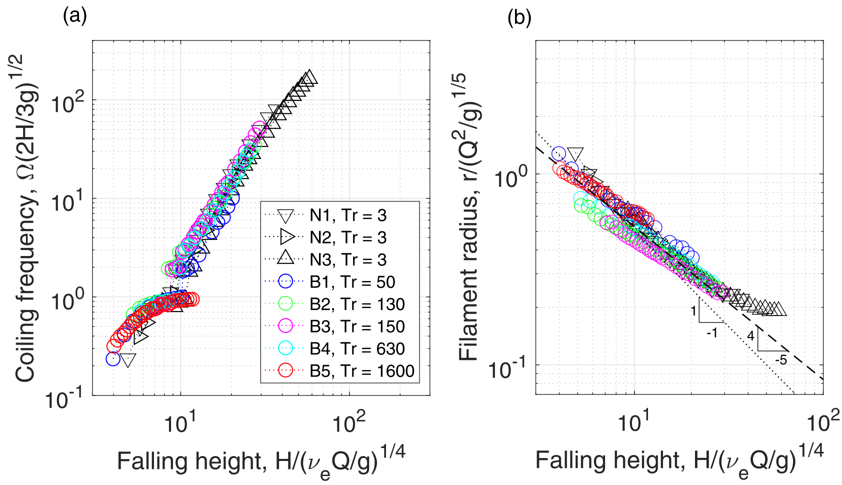

FIG. 5. (a) Filament coiling frequency and (b) filament radius as a function falling height for both Newtonian and viscoelastic fluids: the falling height is normalized by the proposed extensional viscosity (characterized by Trouton ratio, Tr) listed in the figure.

It is important to note that the length scale, $\delta = (\nu Q/g)^{1/4}$, which is based on the force balance of viscous stretching and gravity [5], considers the shear viscosity rather than the extensional viscosity. This is reasonable considering the constant Trouton ratio of 3 for Newtonian fluids. But in the present study with Boger fluids (viscoelastic) we expect the Trouton ratio not to be constant and to be larger than 3. Hence, we propose the use of extensional viscosity, ν_e, instead of shear viscosity, ν, in the length scale, which is

$$\delta_e = (\nu_e Q/g)^{1/4}. \tag{7}$$

However, the extensional viscosity is unknown. Its value can only be measured experimentally with highly specialized equipment (e.g., McKinley and Sridhar [30]). Therefore, we begin our analysis using values in a reverse approach. By adopting the length scale, $\delta_e = (\nu_e Q/g)^{1/4}$, we propose certain extensional viscosity (Trouton ratio) so that the frequency-height curves collapse for both Newtonian and Boger fluids. Figure 5(a) shows a good collapse for all the coiling frequency curves of both Newtonian and Boger fluids using the proposed extensional viscosity listed in the figure. It is to be noted that the proposed Trouton ratio for Boger fluids can be of $O(10^3)$, far larger than that for Newtonian fluids. Similarly, large Trouton ratios have been reported previously in experimental measurements on viscoelastic fluids [29,31].

In addition, using the same extensional viscosity, Fig. 5(b) also shows a good collapse of the filament radius for all the fluids tested. In general, the collapsed filament radius demonstrates a simple monotonic decreasing trend with respect to the falling height, which is in agreement with the results reported in Habibi *et al.* [8]. A unidirectional stretching model was developed by Ribe [5] to describe the filament radius under a strong stretching. In this model, gravity force is balanced by viscous force from extensional stretching and inertia force related to the outlet jetting velocity. According to the model, the slope for the monotonic decreasing curve is -1 [$r \sim H^{-1}$, dotted line in Fig. 5(b)], which is slightly larger than the general trend ($r \sim H^{-4/5}$, dash line) of the collapsed curves.

In the present experimental configuration, the stretching of the filament is a result of the balance between gravity and viscosity. We argue that in the case of viscoelastic fluids, extensional viscosity is more important than shear viscosity. The length scale [Eq. (7)] resulting from the stretching balance successfully collapses the experimental data (Fig. 5), demonstrating the argument above.

Therefore, by using the pendulum frequency scale and the gravity mode length scale, we successfully collapse the frequency-height curves for both Newtonian and Boger fluids with the proposed extensional viscosity. From the derivation of the frequency and length scales, we believe that the frequency jump is an important feature in the coiling frequency performance, and the frequency-height curve can be determined by simply collapsing the frequency jump in both the vertical direction (frequency) and horizontal direction (height). This is in agreement with the experimental results in Mier *et al.* [11] who showed a good collapse of frequency curves by normalizing the falling height with the critical falling height for frequency jump.

Direct measurement of the extensional viscosity and Trouton ratio

Researchers have proposed and used different experimental methods to measure extensional viscosity, as categorized by Petrie [32], including filament stretching rheometer, fiber spinning, stagnation point flows, and converging and contraction flows. One potential issue for those experimental methods, as discussed by Petrie [32], is the controllability of the tested flow. In other words, the fluid flow needs to be steady and spatially uniform for a material rheology test, which is usually difficult to achieve in practical applications. Therefore, the concept of transient extensional viscosity is widely adopted.

As reported by Anna *et al.* [33], the transient extensional viscosity depends on extensional strain (Hencky strain, ϵ) and shows an extensional thickening behavior for dilute polymer solutions: as the Hencky strain increases, the value of the transient extensional viscosity also increases slightly until a critical value of $\epsilon \sim 2$; beyond this value the transient extensional viscosity increases abruptly and remains relatively independent of Hencky strain at $\epsilon \sim 6$, reaching a steady state.

For the experiments conducted here, using the measured filament diameter [33], the Hencky strain can be estimated as

$$\epsilon = -2\ln(2r/d_n), \tag{8}$$

where r is the filament radius and d_n is the nozzle diameter. The Hencky strain for Boger fluids in the current study ranges from about 1.5 (for small falling heights) to 4.5 (for large falling heights), part of which falls below the aforementioned critical Hencky strain of 2. Therefore, the Boger fluids could be expected to have a Trouton ratio ~3 at small falling heights (small Hencky strain) and thus behave similar to Newtonian fluids. However, as shown in Fig. 4, neither the coiling frequency nor the filament radius for the Boger fluids falls on top of the Newtonian counterparts, regardless of falling heights. This discrepancy can be attributed to the fact that the coiling motion of a filament is in a steady state, characterized by a stable coiling frequency and a nearly constant filament diameter. Therefore, the extensional viscosity here affecting the filament coiling performance is steady-state rather than transient extensional viscosity.

To demonstrate that the increased value of extensional viscosity is indeed responsible for the change of the behavior for Boger fluids, we measured the extensional viscosity independently using the Dripping-onto-Substrate (DoS) method [31,34–36] (more details in the Appendix). Three viscoelastic fluids were tested for extensional viscosity and the results are shown in Fig. 6(a). We can see from Fig. 6(a) that the measured Trouton ratio (circles) increases with Hencky strain, which suggests a transient extensional viscosity; a higher polymer concentration leads to a higher Trouton ratio. This trend of Trouton ratio agrees with other experimental measurements of viscoelastic fluids in literature [34]. With that, the proposed Trouton ratio for the coiling experiments (horizontal dash lines) falls close to the measured Trouton ratio at Hencky strain ~4.5 [vertical dotted line in Fig. 6(a)], respectively. As mentioned above, this Hencky strain corresponds to a large falling height in the filament coiling experiments, where the gravity force plays an important role in determining the coiling frequency. From the good agreement between the proposed and measured Trouton ratio, we can ascertain that the change of coiling phenomena of viscoelastic fluids is due to the increased extensional viscosity.

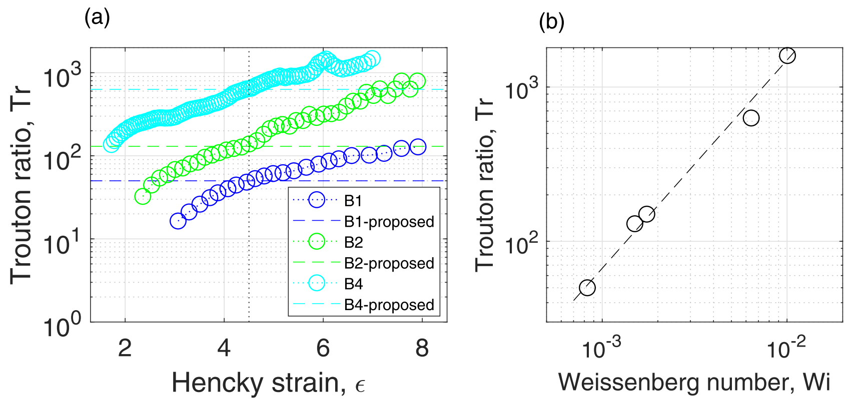

FIG. 6. (a) Independently measured Trouton ratio (circles) as a function of Hencky Strain; the horizontal dash lines show the proposed Trouton ratio for the corresponding fluids, respectively; (b) the Trouton ratio as a function of Weissenberg number.

As is well known, liquid extensional viscosity depends strongly on the polymer concentration of the viscoelastic fluids. The experiments presented here give us an opportunity to analyze this phenomenon from a different perspective. We quantify the polymer concentration effects by the amount of viscoelasticity, quantified by the Weissenberg number, which measures the importance of elastic effects over viscous effects. In this study, the Weissenberg number is defined as

$$\mathrm{Wi} = \frac{\lambda Q}{{d_n}^3}, \tag{9}$$

where λ is the fluid relaxation time, Q is the flow rate and d_n is the nozzle diameter. In Fig. 6(b), we show the measured Trouton ratio as a function of Weissenberg number, Wi. A clear increase of Trouton ratio with Wi is observed, which is expected considering that a higher polymer concentration leads to more elastic contribution to extensional viscosity. The dash line in Fig. 6(b) shows a general increasing trend for the Trouton ratio, which appears to be a power law, $\mathrm{Tr} \sim \mathrm{Wi}^n$, where $n = 1.35$. Clearly, more experiments and modeling are needed to clarify this functional relationship between the extensional viscosity and the Weissenberg number.

Considering the good collapse of coiling frequency and filament radius in Figs. 5(a) and 5(b), we can argue that the experiment of coiling filaments can be used as an alternative way to measure the extensional viscosity of viscoelastic fluids. For a specific flow rate and falling height, the extensional viscosity can be inferred by simply measuring the filament coiling frequency, thus avoiding the use of sophisticated equipment for prescribed uniaxial filament stretching and force measurement.

C. Coiling radius

To further test the efficacy of the length scale using the extensional viscosity, we apply them to analyze the coiling radius R [defined in Fig. 1(a)]. The results are shown in Figs. 7(a) and 7(b). Again, same as the coiling frequency behaviors in Fig. 5, the length scale using extensional viscosity collapses the coiling radius for both Newtonian and Boger fluids [Fig. 7(a)]. We can see that the coiling radius remains more or less constant at very small falling height and then starts to increase until it drops rapidly at a certain falling height $[H/(\nu_e Q/g)^{1/4} \sim 10]$ that corresponds to where the frequency jump happens. Then the coiling radius continues to decrease when further increasing the falling height. This observation is in agreement with both numerical and experimental results of Habibi *et al.* [8]. In addition, these authors argued that the increase of coiling radius corresponds to the start of the inertial-gravitational mode.

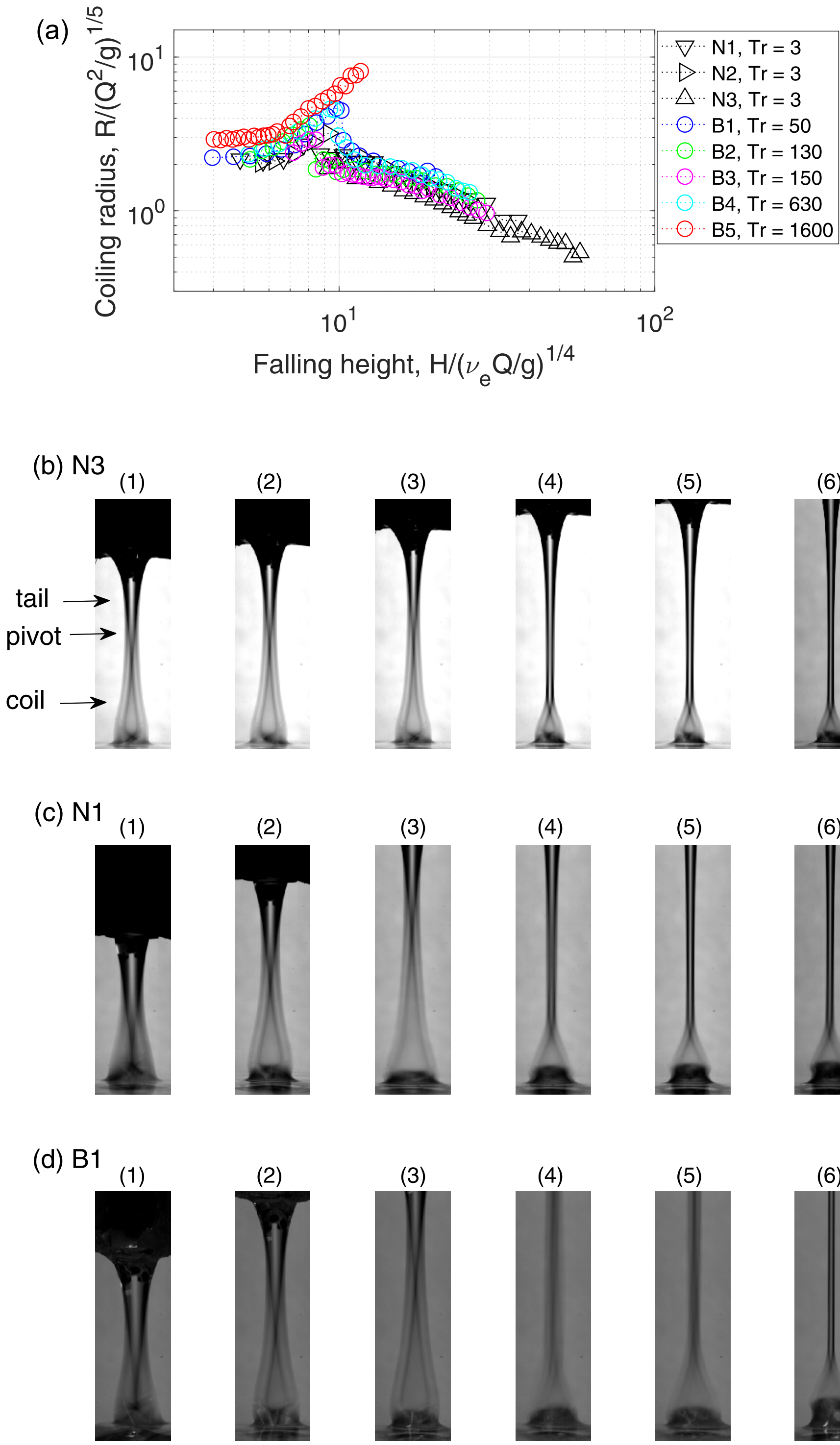

FIG. 7. (a) Coiling radius for both Newtonian and Boger fluids using extensional viscosity in Fig. 5. Filament clouds (overlapping images) near the frequency jump [(3) to (4)]: Newtonian fluids N3 (b), N1 (c), and Boger fluid B1 (d), respectively. The falling height increases from left to right.

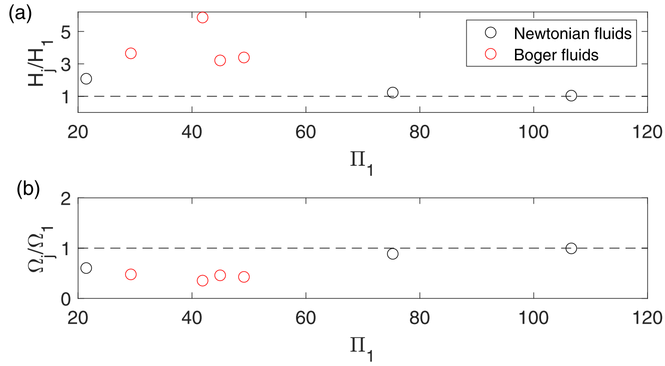

FIG. 8. Comparison of (a) falling height and (b) frequency at the jump between experimental observations (H_j and Ω_j) and predictions (H_1 and Ω_1) using Eqs. (10) and (11).

To further understand the connection between the coiling frequency and the filament coiling radius, we show "averaged" images of coiling filament over multiple cycles to visualize the coiling geometry as shown in Figs. 7(b)–7(d). The blurred part of the image shows the coiling part while the sharp part suggests a steady filament. The point connecting the two parts is the pivot position of the coil (analogous to the pivot point of a pendulum). We can see that from (1) to (3) for all the three cases the pivot position moves upward as the falling height increases. This increasing pivot position corresponds to an increase of coiling radius [Fig. 7(a)]. Then from (3) to (4), the pivot point either moves down to near the bottom plate [Fig. 7(b) (4)] or becomes an unsteady position characterized by a blurred filament tail [Fig. 7(c) (4), 7(d) (4)–(5)]. As the falling height continues to increase, the pivot point stays very stable after the jump for Newtonian fluid N3 [Fig. 7(b) (4)–(6)]; however, for Newtonian fluid N1 and especially Boger fluid B1, a transition region of unsteady coiling exists [Fig. 7(c) (4) and 7(d) (4)–(5)], corresponding to a multifrequency mode after the jump.

This multifrequency mode was also reported in literature for Newtonian fluids [6–8]. However, Mier *et al.* [11] reported no unsteady frequency or looped coiling region in their experiments with honey as testing fluids, similar to the case in Fig. 7(b). Using a numerical approach, Ribe *et al.* [6] showed that this multifrequency coiling region appears only when the nondimensional group Π_1 [Eq. (4)] exceeds a certain critical value Π_1^{crit}. In the present study, Π_1 in Fig. 7(c) (N1 fluid) is larger than the critical Π_1^{crit} while Π_1 in Fig. 7(b) (N3 fluid) is smaller than the critical value, in agreement with the numerical prediction. As for the Boger fluid B1, though Π_1 is smaller than the critical value based on shear viscosity, the unsteady coiling region is evident as shown in Fig. 7(d) (4)–(5). This can be attributed to the large extensional viscosity in Boger fluids that would make the fluid filament more stretch-resistant. Thus, the fluid filament behaves more like an elastic whirling string that can induce resonance phenomenon in the inertial-gravitational mode [6].

In particular, using the same length scale in Eq. (6), Ribe *et al.* [6] numerically predicted the falling height for the frequency jump as

$$H_1 = 2.58(\nu^9 Q/g^5)^{1/16}. \tag{10}$$

And the corresponding frequency is given as

$$\Omega_1 = 0.834(g^{21}/\nu^9 Q)^{1/32}. \tag{11}$$

In the current study, Fig. 8 shows the comparison between the predicted jump height and frequency [Eqs. (10) and (11)] and the experimental results for both Newtonian and Boger fluids. In general, the jump frequency comparison shows a better agreement between experimental observation and predicted results than the falling height comparison. This is in agreement with the observations in Ribe *et al.* [6], and the authors argued that one possible reason for it can be that the coiling frequency is not sensitive to the change of falling height within the multifrequency region around the frequency jump. For comparison between Newtonian and Boger fluids as shown in Fig. 8, the prediction works better for Newtonian fluids for both falling height and coiling frequency. In particular, for Newtonian fluids, the prediction has better agreement with experiments especially when the nondimensional group Π_1 becomes larger.

IV. CONCLUSIONS

We have experimentally investigated the viscous filament coiling of Newtonian and Boger (viscoelastic) fluids. To our knowledge, coiling for viscoelastic fluids had not been analyzed in sufficient detail. We found that the coiling frequency curves of different Newtonian fluids collapsed well considering a pendulum frequency scale and a length scale related to the gravitational mode. Then we extended the scaling to Boger fluids and found that the extensional viscosity, instead of shear viscosity, is more appropriate to calculate the length scale to characterize the coiling performance of Boger fluids. Using the extensional viscosity of the Boger fluids, we have demonstrated a good collapse of the coiling frequency curves, the filament radius and the coiling radius curves for both Newtonian and Boger fluids. The inferred values of the extensional viscosity were in very good agreement with the measurements using the DoS method.

With a similar shear viscosity to Newtonian fluids but a large extensional viscosity, Boger fluids are found to resist the gravitational stretching and significantly reduce the coiling frequency, which could indicate a better control for some industrial processes. In the measurement of rheological properties, the filament coiling process can be a potential method to determine the extensional viscosity considering the collapse of coiling frequency curve with respect to the length scale using extensional viscosity.

ACKNOWLEDGMENTS

B.P. acknowledges the financial support of Conacyt-Mexico for his graduate fellowship. The financial support of FONCA-Mexico (Grant No. CNCA.FONCA.04S.04.ACT.IN.ACT.030.18) is greatly acknowledged.

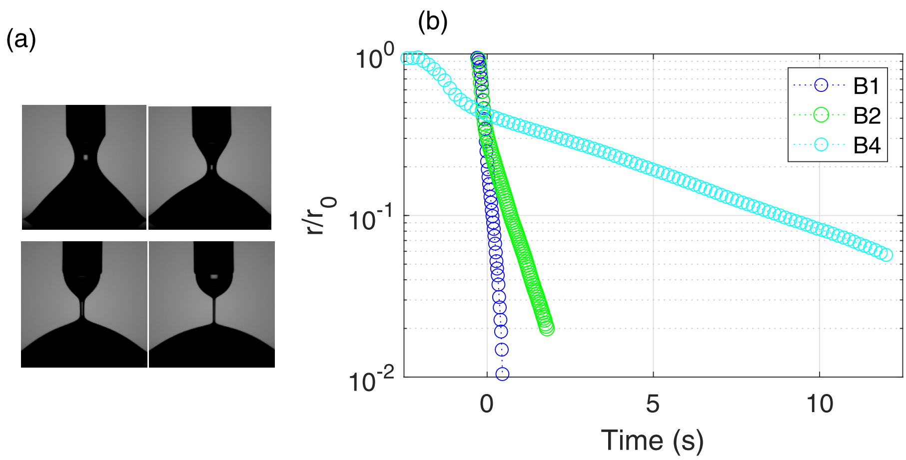

FIG. 9. (a) Sequence of sample images showing the thinning fluid bridge between the nozzle and the substrate sessile drop; (b) radius evolution of the fluid bridge in time for three tested fluids, filament radius normalized by nozzle radius r_0.

APPENDIX: MEASUREMENT OF THE EXTENSIONAL VISCOSITY

We measured the extensional viscosity using the Dripping-onto-Substrate (DoS) method [34]. In this method, the testing fluid drips from a nozzle onto a substrate forming a thinning fluid bridge between the nozzle and the deposited sessile drop. The thinning process of the fluid bridge is recorded using a camera as shown in Fig. 9(a). Typically the evolution of the radius can be divided into two regimes: inertial-capillary regime [time < 0 in Fig. 9(b)] and elastocapillary regime [time > 0 in Fig. 9(b)]. In the elastocapillary regime, the surface tension is balanced by the force due to the extensional stretching of the fluid filament. Using this force balance, the extensional viscosity μ_e is thus evaluated as

$$\mu_e = \frac{\sigma}{\dot{\epsilon} r} = \frac{\sigma}{-2dr/dt}, \tag{A1}$$

where σ is the surface tension of the fluid, r is the radius of the fluid bridge in the elastocapillary regime, $\dot{\epsilon} = -2d \ln r/dt$ is the extension rate of the fluid bridge.

Using this method, three viscoelastic fluids (B1, B2, and B4) were tested and the thinning radius of the fluid bridge is shown in Fig 9(b). Using Eq. (A1) in the elastocapillary regime [time > 0 in Fig 9(b)], the extensional rate $\dot{\epsilon}$ of the fluid bridge can be calculated, thus the extensional viscosity and the Trouton ratio can be evaluated for each tested fluid as shown in Fig. 6(a).

[1] G. Barnes and R. Woodcock, Liquid rope-coil effect, Am. J. Phys. **26**, 205 (1958).

[2] G. I. Taylor, Instability of jets, threads, and sheets of viscous fluid, in *Applied Mechanics: International Union of Theoretical and Applied Mechanics*, edited by M. Hetenyi and W. G. Vincente (Springer, Berlin, 1969).

[3] B. Tchavdarov, A. L. Yarin, and S. Radev, Buckling of thin liquid jets, J. Fluid Mech. **253**, 593 (1993).

[4] J. O. Cruickshank, Viscous jet buckling: A theoretical and experimental analysis with extension to general fluid stability, Ph.D. thesis, Iowa State University, Ames, IA, 1980.

[5] N. M. Ribe, Coiling of viscous jets, Proc. R. Soc. A **460**, 3223 (2004).

[6] N. M. Ribe, H. E. Huppert, M. A. Hallworth, M. Habibi, and D. Bonn, Multiple coexisting states of liquid rope coiling, J. Fluid Mech. **555**, 275 (2006).

[7] M. Maleki, M. Habibi, R. Golestanian, N. M. Ribe, and D. Bonn, Liquid Rope Coiling on a Solid Surface, Phys. Rev. Lett. **93**, 214502 (2004).

[8] M. Habibi, M. Maleki, R. Golestanian, N. M. Ribe, and D. Bonn, Dynamics of liquid rope coiling, Phys. Rev. E **74**, 066306 (2006).

[9] N. M. Ribe, M. Habibi, and D. Bonn, Liquid rope coiling, Annu. Rev. Fluid Mech. **44**, 249 (2012).

[10] N. M. Ribe, Liquid rope coiling: A synoptic view, J. Fluid Mech. **812**, R2 (2017).

[11] F. A. Mier, R. Bhakta, N. Castano, J. Garcia, and M. J. Hargather, Experimental measurement of steady and transient liquid coiling with high-speed video and digital image processing, Fluids **3**, 107 (2018).

[12] S. Chiu-Webster and J. R. Lister, The fall of a viscous thread onto a moving surface: A fluid-mechanical sewing machine, J. Fluid Mech. **569**, 89 (2006).

[13] S. W. Morris, J. H. P. Dawes, N. M. Ribe, and J. R. Lister, Meandering instability of a viscous thread, Phys. Rev. E **77**, 066218 (2008).

[14] B. Palacios, A. Rosario, M. M. Wilhelmus, S. Zetina, and R. Zenit, Pollock avoided hydrodynamic instabilities to paint with his dripping technique, Plos One **14**, e0223706 (2019).

[15] A. Kaye, A bouncing liquid stream, Nature **197**, 1001 (1963).

[16] A. A. Collyer and P. J. Fisher, The Kaye effect revisited, Nature **261**, 682 (1976).

[17] M. Versluis, C. Blom, D. van der Meer, K. van der Weele, and D. Lohse, Leaping shampoo and the stable Kaye effect, J. Stat. Mech. (2006) P07007.

[18] J. M. Binder and A. J. Landig, The Kaye effect, Eur. J. Phys. **30**, S115 (2009).

[19] T. Majmudar, M. Varagnat, W. Hartt, and G. McKinley, Nonlinear dynamics of coiling in viscoelastic jets, arXiv:1012.2135.

[20] D. V. Boger, A highly elastic constant-viscosity fluid, J. Non-Newtonian Fluid Mech. **3**, 87 (1977).

[21] R. J. Binnington and D. V. Boger, Constant viscosity elastic liquids, J. Rheol. **29**, 887 (1985).

[22] N. C. Keim, M. Garcia, and P. E. Arratia, Fluid elasticity can enable propulsion at low reynolds number, Phys. Fluids **24**, 081703 (2012).

[23] M. Dasgupta, B. Liu, H. C. Fu, M. Berhanu, K. S. Breuer, T. R. Powers, and A. Kudrolli, Speed of a swimming sheet in newtonian and viscoelastic fluids, Phys. Rev. E **87**, 013015 (2013).

[24] R. I. Tanner and S. Dai, Rheology of noncolloidal suspensions with corn syrup matrices, Rheol. Acta **55**, 739 (2016).

[25] A. Castillo, W. L. Murch, J. Einarsson, B. Mena, E. S. G. Shaqfeh, and R. Zenit, Drag coefficient for a sedimenting and rotating sphere in a viscoelastic fluid, Phys. Rev. Fluids **4**, 063302 (2019).

[26] M. N. Ribe, M. Habibi, and D. Bonn, Stability of liquid rope coiling, Phys. Fluids **18**, 084102 (2006).

[27] L. Mahadevan, W. S. Ryu, and A. D. T. Samuel, Fluid "rope trick" investigated, Nature **392**, 140 (1998).

[28] M. J. Blount, Bending and buckling of a falling viscous thread, Ph.D. thesis, University of Cambridge, Cambridge, UK, 2010.

[29] G. H. McKinley, S. H. Spiegelberg, S. L. Anna, and M. Yao, Extensional rheometry of polymer solutions and the uniaxial elongation of viscoelastic filaments, in *Proceedings of the 4th Microgravity Fluid Physics & Transport Phenomena Conference* (Office of Life and Microgravity Science & Applications, NASA, Cleveland Ohio, 1998), pp. 1–14.

[30] G. H. McKinley and T. Sridhar, Filament-stretching rheometry of complex fluids, Annu. Rev. Fluid Mech. **34**, 375 (2002).

[31] J. Dinic, L. N. Jimenez, and V. Sharma, Pinch-off dynamics and dripping-onto-substrate (DoS) rheometry of complex fluids, Lab on a Chip **17**, 460 (2017).

[32] C. J. S. Petrie, Extensional viscosity: A critical discussion, J. Non-Newtonian Fluid Mech. **137**, 15 (2006).

[33] S. L. Anna, G. H. McKinley, D. A. Nguyen, T. Sridhar, S. J. Muller, J. Huang, and D. F. James, An interlaboratory comparison of measurements from filament-stretching rheometers using common test fluids, J. Rheol. **45**, 83 (2001).

[34] J. Dinic, Y. Zhang, L. N. Jimenez, and V. Sharma, Extensional relaxation times of dilute, aqueous polymer solutions, ACS Macro Lett. **4**, 804 (2015).

[35] B. Keshavarz, V. Sharma, E. C. Houze, M. R. Koerner, J. R. Moore, P. M. Cotts, P. Threlfall-Holmes, and G. H. McKinley, Studying the effects of elongational properties on atomization of weakly viscoelastic solutions using Rayleigh Ohnesorge Jetting Extensional Rheometry (ROJER), J. Non-Newtonian Fluid Mech. **222**, 171 (2015).

[36] J. Dinic, M. Biagioli, and V. Sharma, Pinch-off dynamics and extensional relaxation times of intrinsically semi-dilute polymer solutions characterized by dripping-onto-substrate rheometry, J. Polym. Sci., Part B: Polym. Phys. **55**, 1692 (2017).